Water in star-forming regions with *Herschel*[*]

L.E. Kristensen[1] and **E.F. van Dishoeck**[1,2,**]

[1] Leiden Observatory, Leiden University, PO Box 9513, 2300 RA Leiden, The Netherlands
[2] Max Planck Institut für Extraterrestrische Physik, Giessenbachstrasse 1, 85748 Garching, Germany

The *Herschel Space Observatory* is well suited to address several important questions in star- and planet formation, as is evident from its first year of operation. This paper focuses on observations of water, a key molecule in the physics and chemistry of star-formation. In the WISH Key Program, a comprehensive set of water lines is being obtained with the HIFI and PACS instruments toward a large sample of well-characterized protostars, covering a wide range of luminosities and evolutionary stages. Lines of H_2O, CO and their isotopologues, as well as chemically related hydrides, [O I] and [C II] are observed. Together, the data determine the abundance of water in cold and warm gas, reveal the entire CO ladder up to 4000 K above ground, elucidate the physical processes responsible for the warm gas (passive heating, UV or X-ray-heating, shocks), quantify the main cooling agents, and probe dynamical processes associated with forming stars and planets.

1 Introduction

Water is a key molecule in the formation of stars and planetary systems, both as a cornerstone molecule in the oxygen chemistry and as a diagnostic of the physical structure of young stellar objects (YSOs). It is thus important to follow the abundance and excitation of water from the earliest stages of the collapsing cloud to the end stages of planet-forming disks (see e.g., reviews by Cernicharo & Crovisier 2005 and Melnick 2009). The Herschel Key Program "Water in star-forming regions with Herschel" (WISH; van Dishoeck et al. 2011) uses high spectral and spatial resolution HIFI and PACS observations of water through all evolutionary stages of star formation to follow the "water trail" and to use water as a probe of physical and dynamical processes taking place.

Previous data have suggested that the abundance of water is very low, 10^{-9}–10^{-8}, in the cold quiescent parts of the molecular envelope, where the bulk of water is in the form of ice on dust grains. As the temperature increases closer to the protostar, all water is expected to evaporate and the abundance to increase by several orders of magnitude, up to $\sim 10^{-5}$–10^{-4} with respect to H_2. Water is also frozen out onto dust grains in shocks, but sputtering of the grain mantles effectively releases all water into the gas phase. At the same time, atomic oxygen may be pushed into water through neutral-neutral reactions in the warm post-shock gas. Both processes lead to a jump in the abundance by up to four orders of magnitude, to $\sim 10^{-4}$, and this variation makes water such an excellent diagnostic of energetic phenomena. These processes have been previously inferred by a combination of SWAS and ISO data (e.g., Boonman et al. 2003). SWAS was able to spectrally resolve the H_2O 1_{10}–1_{01} transition at 557 GHz (Bergin et al. 2003, Franklin et al. 2008), but in a much larger beam and at a lower sensitivity than what is currently possible with the Heterodyne Instrument for the Far-Infrared on *Herschel*. These factors make it possible to detect water in a larger number of protostars at any evolutionary stage, as well as detecting higher-excited lines and the rare isotopologue $H_2^{18}O$.

2 Observational strategy

The Heterodyne Instrument for the Far-Infrared (HIFI; de Graauw et al. 2010) is used as the instrument of choice for observing water. Because of its high spectral resolution and sensitivity, it is possible to resolve the line profiles down to a velocity resolution of < 0.1 km s^{-1}. Depending on the type of object, up to ten H_2O and isotopologue transitions are targeted with HIFI, the transitions having upper-level energies of 50 – 500 K above the ground-state. For the faintest objects (pre-stellar cores and protoplanetary disks), the integration time is long enough (up to 10 hours or more) that an rms of $\sim$ 1 mK is achieved in the H_2O 1_{10}–1_{01} and 1_{11}–0_{00} ground state lines, thus representing the longest single-pointing integrations done with HIFI. The bulk of the observations are carried out as single-pointing observations with beam-sizes ranging from 12″ at 1834 GHz to 39″ at 557 GHz. $H_2^{18}O$ and $H_2^{17}O$ lines are targeted to constrain the optical depth of emission lines across the entire mass spectrum

---

and in protostellar outflows. High-J CO and isotopologue lines are also targeted up to J=10–9 ($E_{\rm up}$ = 300 K).

HIFI observations are complemented by data from the Photodetector Array Camera and Spectrometer (PACS; Poglitsch■ et al. 2010). PACS has a resolving power of only 1500-4000 and does not generally resolve the line profiles. However, its 5×5 array receiver with 9.4″ pixels provides spatial information. Full spectral scans are carried out for a small number of low- and high-mass YSOs, whereas line scans of a specific sub-set of lines are done for the entire mass spectrum of sources. The lines targeted include high-J CO lines, OH, [O I] at 63 and 145 μm, and, of course, higher excited H_2O lines (up to $E_{\rm up} \sim 1000$ K). Fully sampled line maps are obtained for three protostellar outflows in the 179.5 μm H_2O line (2_{12}–1_{01}).

WISH targets about 80 sources, most of them in the embedded phase of star formation. The luminosity of the YSOs ranges from < 1 L$_\odot$ to $> 10^5$ L$_\odot$, covering low-, intermediate- and high-mass star formation. A few pre-stellar cores and protoplanetary disks are included in the sample to probe the different evolutionary stages from the pre-collapse stage of the cloud to the phase when the envelope has been dispersed and only a young star with a disk is left. The full source list and associated line list can be found in van Dishoeck et al. (2011).

3 Results

Figure 1 shows the evolution of the H_2O 1_{10}–1_{01} line at 557 GHz from the pre-stellar core B68 (Caselli et al. 2010), to the low-mass embedded source NGC1333-IRAS4A (Kristensen et al. 2010) ending with the protoplanetary disk DM Tau (Bergin et al. 2010). This temporal evolutionary sequence highlights that during the quiescent phases of star formation, the water abundance is very low. The embedded stage of star formation, however, shows very broad and complex line profiles consisting of many dynamical components. An example is emission from the low-mass source NGC1333-IRAS4A, which shows a broad underlying component centered at the source velocity with an inverse P-Cygni profile on top indicative of large-scale in-fall. In disks,■ again most of the water is frozen out onto grains.

The mass-evolutionary track is very different from the temporal track. Comparing typical low-, intermediate, and high-mass YSOs (Fig. 2) shows that absolute intensity aside,■ the profiles are remarkably similar. They are all broad, complex and consist of multiple components, clearly indicating that the water emission is primarily generated in shocks. In the following, the initial results from each sub-program of WISH are summarized.

3.1 Pre-stellar cores

Caselli et al. (2010) present early results for the two cores L1544 and B68, with the B68 o-H_2O $1_{10} - 1_{01}$ spectrum included in Fig. 1. These spectra took $\sim$4 hr integration
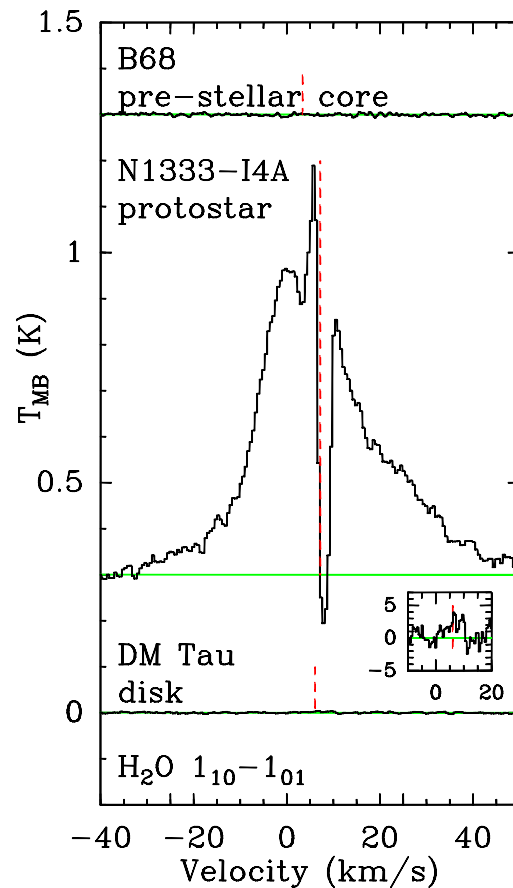

Fig. 1 Evolution of the H_2O 1_{10}–1_{01} line at 557 GHz for the pre-stellar core B68, the low-mass embedded YSO NGC1333-IRAS4A and the protoplanetary disk DM Tau. The red dashed line indicates the systemic velocity, and the inset shows the tentative detection of H_2O in a disk. Water emission is only bright in the embedded phase of star formation.

(on+off) each. No emission is detected in B68 but interestingly, the L1544 spectrum shows a tentative *absorption* feature against the submillimeter continuum at velocities where the CO 1–0 line is seen in emission. The B68 limit down to 2.0 mK rms in 0.6 km s^{-1} bins is more than an order of magnitude lower than the previous upper limit obtained by SWAS for this cloud (Bergin & Snell 2002) as well as most pre-*Herschel* model predictions. The 3σ upper limit corresponds to an o−H_2O column density $< 2.5 \times 10^{13}$ cm^{-2} and a mean line-of-sight abundance $< 1.3 \times 10^{-9}$. If the water absorption in L1544 is confirmed by deeper integrations currently planned within WISH, it provides a very powerful tool to determine the water abundance profile along the line of sight.
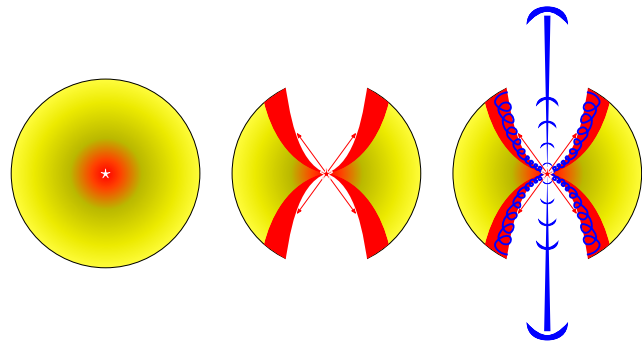
3.2 Low-mass YSOs

The embedded low-mass sources are often dominated by outflows (see, e.g., Arce et al. 2007 for a recent review). $H_2^{16}O$ emission is detected towards all sources, both Class 0 and the more evolved Class I (Fig. 3; Kristensen et al. in prep.). These results constitute the first detection of cold
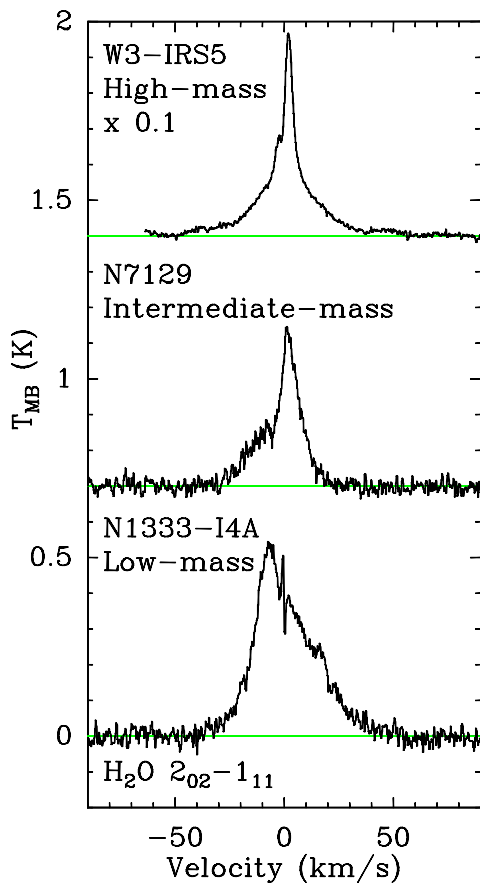
Fig. 2 Evolution of the H_2O 2_{02}–1_{11} line at 988 GHz for the high-mass YSO W3-IRS5, the intermediate-mass YSO NGC7129-IRS1 and the low-mass YSO NGC1333-IRAS4A. The line centers have been shifted to 0 km s^{-1}. Note the presence of broad (FWHM $\geq$25 km s^{-1} and medium-broad (FWHM $\approx$5–10 km s^{-1}) components in all sources irrespective of luminosity, as well as inverse P-Cygni profile on top of the broad line in NGC1333-IRAS4A.

Fig. 4 Cartoons showing the different physical components of a protostar on scales of a few thousand AU. (Left) The molecular envelope heated by the accretion luminosity of the protostar. (Center) Outflow cavity walls heated by UV photons from the protostar. (Right) Shell shocks running along the outflow cavity walls and molecular jet with internal working surfaces (R. Visser, priv. comm.).

H_2O in a Class I object as well as the detection of cold $H_2^{18}O$ in a low-mass protostar. The line profiles appear to be unique to each source, with very few common traits. The main characteristic of all detected H_2O lines, including the $H_2^{18}O$ isotopologue lines, is the width of the line profiles. It is typically > 20 km s^{-1}, but may go up to > 50 km s^{-1}. The profiles show many dynamical components, including inverse P-Cygni-type profiles, emission from molecular "bullets" at high velocities, and deep absorptions going below the continuum level. The $H_2^{18}O$ transition is also self-absorbed, indicating that the envelope is optically thick even in $H_2^{18}O$.

The bulk of H_2O emission arises in shocks associated with the molecular outflows (Kristensen et al. 2010), and the water abundance is found to increase with velocity up to H_2O/CO abundance ratios of ~ 1. The only clear signature of the envelope is the deep absorption by gas-phase water in the outer, cold envelope, where the abundance is constrained to $\sim 10^{-8}$. The lack of any envelope emission signature, in particular the absence of excited $H_2^{18}O$ emission, is used to constrain the inner envelope abundance to $< 10^{-5}$ (Visser

et al. in prep.). This upper limit is significantly lower than expected if all of the water ice on grains evaporates in the inner envelope.

The next step consists of detailed 2D modeling for each protostar. Such a model has already been developed and tested for the low-mass protostar HH46 (van Kempen et al. 2010, Visser et al. in prep.). The model consists of three separate physical components: the molecular envelope heated by the accretion luminosity of the protostar, UV-heating of the outflow cavity walls and shocks along the cavity walls (see Fig. 4). The 'passively-heated' model uses the DUSTY radiative transfer code to compute the temperature structure through the envelope for a given power-law density structure, and assumes that the gas temperature is equal to the dust temperature. The UV model adds a photon-heated gas layer along the outflow cavity walls, either using a parametrized temperature grid based on the PDR models of Kaufman et al. (1999) or by computing the gas temperature explicitly in a 2D code such as presented by Bruderer et al. (2010). The line emission from the combined passively heated and photon-heated models is then computed using the radiative transfer code LIME (Brinch & Hogerheijde 2010). Shocks are added using the model results from Kaufman & Neufeld (1996). With this model it is possible to reproduce the CO ladder from J=2–1 up to J=40–39 with only two free parameters: the UV luminosity from the source and the shock velocity, as shown in Fig. 5. The passively heated envelope reproduces the low-J lines ($\leq$6), the UV-heated layer the intermediate-J lines ($J \approx$10–20), and the shocks the high-J lines ($J \geq 20$). Although there is some degeneracy in the models resulting in uncertainties in the inferred values of these two parameters, the conclusion that both components are needed is robust. Work is currently underway to do the same for H_2O.
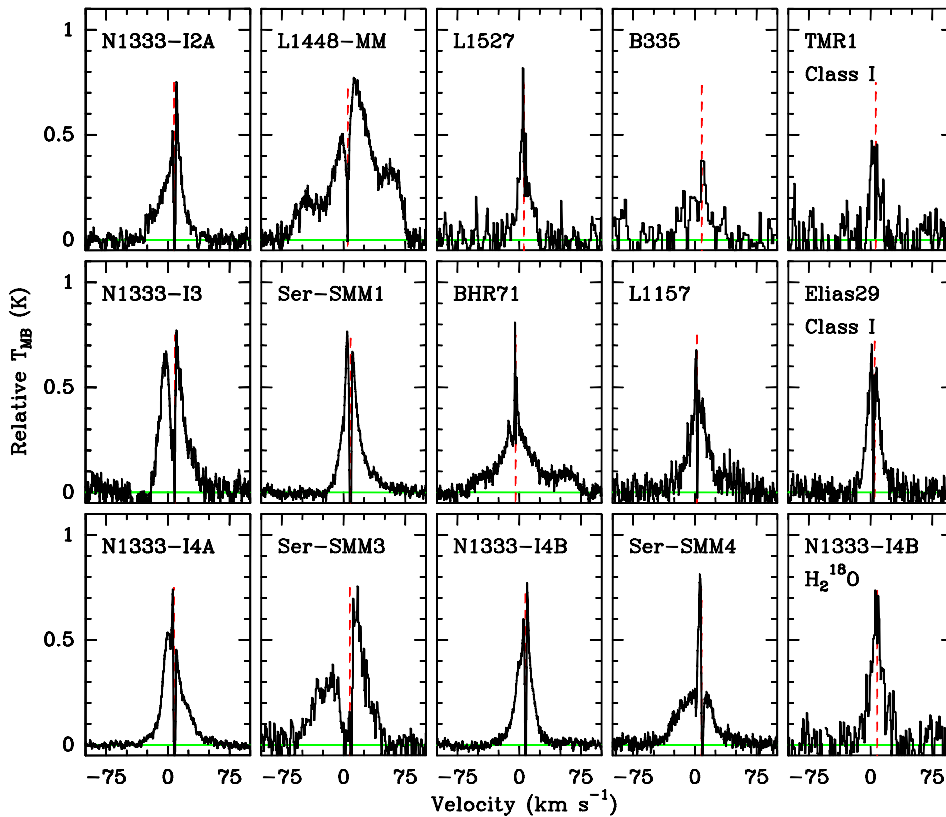
Fig. 3 HIFI spectra of a selection of low-mass Class 0 and I sources in the H_2O $1_{10}-1_{01}$ transition at 557 GHz. The spectra have been scaled to a peak intensity of 0.8 K. The lower right panel shows the detection of the $H_2^{18}O$ $1_{10}-1_{01}$ transition towards the embedded class 0 source NGC1333-IRAS4B. All spectra are continuum-subtracted and the red dashed line indicates the source velocity.
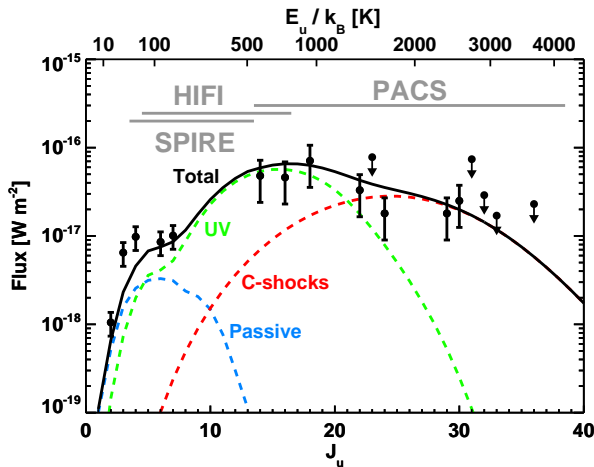
Fig. 5 CO ladder for the embedded low-mass protostar HH46. The ladder is decomposed into three components arising from the passively heated envelope, UV heating of the outflow cavity walls, and shell shocks running along the cavity walls. The wavelength ranges of the three instruments on-board *Herschel* are shown.

3.3 Intermediate-mass YSOs

Observations of various water lines toward NGC 7129 FIRS2 (430 $L_\odot$, 1260 pc) are presented in Fich et al. (2010) and Johnstone et al. (2010) and one of the excited $p-H_2O$ lines detected with HIFI is included in Fig. 2. The line profile is

similar to that of the low-mass YSO NGC 1333 IRAS4A, showing both a broad component (FWHM $\sim$25 km s^{-1}) due to shocks along the outflow cavity as well as a medium-broad component (FWHM $\sim$6 km s^{-1}) associated with small-scale shocks in the inner dense envelope. Quantitative analysis of all the H_2O and isotopologue lines observed for this object result in an outer envelope abundance X_D of order $\sim 10^{-7}$, an order of magnitude higher than for the low- and high-mass YSOs. Alternatively, both the high-J CO and H_2O lines seen with HIFI and PACS can be analyzed in a single slab model with a temperature of ~ 1000 K and density $\sim 10^7 - 10^8$ cm^{-3}, representative of a shock in the inner dense envelope (Fich et al. 2010). This leads to a typical H_2O/CO abundance ratio of 0.2–0.5.

3.4 High-mass YSOs

Figure 2 includes the excited $p-H_2O$ line for the high-mass YSO W3 IRS5 (Chavarría et al. 2010). The profile reveals the same broad and medium-broad components as seen for their low- and intermediate-mass counterparts. In addition to self-absorption and absorption of the cold envelope against the continuum, absorptions due to foreground clouds lying along the line of sight are seen at various velocities. In particular, the high S/N absorption data of the ground-state $p-H_2O$ line show cold clouds surrounding the protostellar
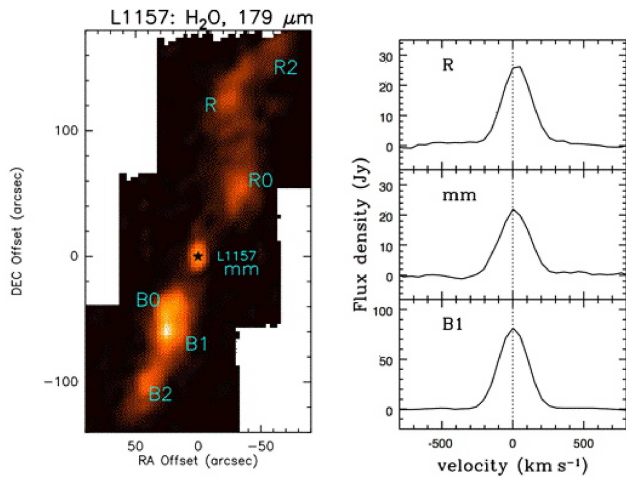
Fig. 6   Map of the L1157 outflow in the H_2O $2_{12}-1_{01}$ transition at 179.5 μm obtained with PACS (left). Three representative spectra are shown to the right from the red outflow lobe (R), the source position (mm) and the blue outflow lobe (B1). The lines are unresolved.

envelope at nearby velocities, revealing the detailed structure of the protostellar environment (Marseille et al. 2010). Broad line profiles due to outflows associated with the high-mass protostars are commonly seen, testifying to the importance of shocks. Moreover, the presence of blue-shifted absorption suggests expansion of the outer envelope rather than infall.

The different physical components composing the high-mass protostellar environment can be disentangled to first order with simple models, as demonstrated by initial performance verification data on DR21 (OH) (van der Tak et al. 2010). Using a slab model and assuming an o/p ratio of 3, the broad component due to the outflow is found to have an H_2O abundance of a few $\times 10^{-6}$. Water is much less abundant in the foreground cloud where $p-H_2O$ has an abundance of 4×10^{-9}. The outer envelope abundance is even lower, a few $\times 10^{-10}$.

3.5   Outflows

Figure 6 shows the Herschel-PACS image of H_2O in the 179 μm line toward the Stage 0 source L1157 obtained during the science demonstration phase of *Herschel* (Nisini et al. 2010). The map clearly reveals where the shocks interact with the molecular cloud, lighting up the water emisson along the outflow. The H_2O emission is spatially correlated with that of pure rotational lines of H_2 observed with *Spitzer* (Neufeld et al. 2009), and corresponds well with the peaks of other shock-produced molecules such as SiO and NH_3 along the outflow. In contrast with these species, H_2O is also strong at the source position itself. The analysis of the H_2O 179 μm emission, combined with existing Odin and SWAS data, shows that water originates in warm compact shocked clumps of a few arcsec in size, where the water abundance is of the order of 10^{-4}, i.e., close to that expected from high-

temperature chemistry. The total H_2O cooling amounts to 23% of the total far-IR energy released in shocks estimated from the ISO-LWS data (Giannini et al. 2001).

The PACS spectra contained in Figure 6 are spectrally unresolved. HIFI spectra of H_2O and CO at the B1 position in the blue outflow lobe (see Fig. 6) have been presented and analyzed by Lefloch et al. (2010) as part of the CHESS key program, showing that the H_2O abundance increases with shock velocity. They propose that this reflects the two mechanisms for producing H_2O: ice evaporation at the lower velocities and high temperature chemistry at the higher velocities where the $O + H_2$ and $OH + H_2$ reactions become significant. The presence of NH_3 (another grain surface product) in only the lower velocity gas is consistent with this picture (Codella et al. 2010), but other explanations are not excluded.

3.6   Radiation diagnostics

An early surprise from all *Herschel*-HIFI key programs is the detection of widespread H_2O^+ absorption in a variety of galactic sources including diffuse clouds, the envelopes of massive YSOs and outflows (see, e.g., Gerin et al. 2010). H_2O^+ and OH^+ lines are even seen in emission in SPIRE-FTS spectra of the AGN Mkr231 (van der Werf et al. 2010).

Within WISH, several hydride molecules have been targeted explicitly as diagnostics of the presence of UV radiation and/or X-rays deep inside the envelope from which the radiation cannot be observed directly due to the large extinction. Pre-*Herschel* models had predicted the importance of species like OH^+, H_2O^+, SH^+ and CH^+ in probing this radation (e.g., Stäuber et al. 2004, 2005, 2007). Subsequent models have also highlighted the importance of the 2D geometry and UV-illuminated cavity walls in producing these species (Bruderer et al. 2010). Deep HIFI integrations on two high-mass YSOs reveal indeed most of these molecules, a confirmation of the model results. CH, NH, OH^+ and H_2O^+ are detected toward both W3 IRS5 and AFGL 2591 (Benz et al. 2010; Bruderer et al. 2010). In addition SH^+ and H_3O^+ are seen toward W3 and CH^+ toward AFGL 2591. Only SH and NH^+ are not detected. H_2O^+, OH^+ and SH^+ are new molecules, with OH^+ and SH^+ only recently detected for the first time in ground-based APEX observations by Wyrowski et al. (2010) and Menten et al. (2011), respectively.

The observed range in line profiles and excitation conditions (absorption versus emission) immediately indicates that the species originate in different parts of the YSO environment. The OH^+/H_2O^+ abundance ratio of > 1 for the blue-shifted gas seen in absorption in both sources indicates low density and high UV fields (Gerin et al. 2010), as expected along the cavity walls at large distances from the source. Low densities ($< 10^4$ cm^{-3}) and a low molecular fraction (i.e., a H_2/H ratio of a few %) are needed to prevent H_2O^+ from reacting rapidly with H_2 to form H_3O^+.

The CH, CH^+ and H_3O^+ emission lines must arise closer to the protostar, at densities $> 10^6$ cm^{-3} (Bruderer et al.

2010). Their abundances are roughly consistent with the 2D photochemical models, in which high temperature chemistry and high UV fluxes boost their abundances along the outflow walls (Bruderer et al. 2009, 2010). The UV field is enhanced by at least four orders of magnitude compared with the general interstellar radiation field in these regions.

Because the H_2O^+ ground state line occurs close to that of $p-H_2O$, observations of both species are available for a large sample of high-mass protostars within WISH. Using also $H_2^{18}O$ data, Wyrowski et al. (2010) provide column densities for both species for all components along 10 lines of sight. H_2O^+ is always in absorption, even when H_2O is seen in emission. Overall, H_2O^+/H_2O ratios range from 0.01 to > 1, with the lower values found in the dense protostellar envelopes and the larger values in diffuse foreground clouds and outflows, as expected from the above mentioned models.

3.7 Disks

Deep integrations on the DM Tau disk show a tentative detection of the $o-H_2O$ line with a peak temperature of $T_{MB}=2.7$ mK and a width of 5.6 km s^{-1} (Bergin et al. 2010). Whether detected or not, the inferred column density is a factor of 20–130 weaker than predicted by a simple model in which gaseous water is produced by photodesorption of icy grains in the UV illuminated regions of the disk (Dominik et al. 2005). The most plausible implication of this lack of water vapor is that more than 95-99% of the water ice is locked up in coagulated grains that are so large that they are not cycled back up to the higher disk layers but remain settled in the midplane.

4 Conclusions

The initial results of the WISH program show that water and related species can indeed be used as physical and chemical probes of star-forming regions. Water shows large abundance variations between cold and warm gas, with abundances of gaseous water in pre-stellar cores and disks even lower than most pre-*Herschel* predictions. In contrast, shocks are seen brightly in broad water emission lines, obscuring any narrower emission from quiescent hot cores, even in isotopologue lines. Ions and hydrides involved in the water chemistry schemes are surprisingly easy to detect and are found to be widely distributed throughout the interstellar medium. The CO ladder, with detections of lines as high as J=44–43, forms a powerful tool to unravel the physical components of the protostellar envelope. Observations of all major coolants allow the total far-infrared cooling to be quantified. So far, water has not yet been found to be the major coolant in any of these regions.

Quantitative analysis of *Herschel* data will require the further development of multidimensional models of protostellar envelopes, outflows and disks. Together with the results from related *Herschel* key programs, they will greatly enhance our understanding of water in the galactic interstellar medium and solar system, and provide a true legacy for decades to come. Eventually, they will allow the determination of the formation and destruction of water from the most diffuse gas to planet-forming disks, and eventually comets and planets in our own Solar system.

References

Aikawa, Y., Herbst, E., Roberts, H., & Caselli, P. 2005, ApJ, 620, 330

Arce, H.G., Shepherd, D., Gueth, F. et al. 2007, Protostars and Planets V, 245

Benz, A. O., et al. 2010, A&A, 521, L35

Bergin, E.A., Hogerheijde, M.R., Brinch, C. et al. 2010, A&A, 521, L33

Bergin, E.A., Kaufman, M.J., Melnick, G.J. et al. 2003, ApJ, 582, 830

Bergin, E.A., & Snell, R. L. 2002, ApJL, 581, L105

Boonman, A.M.S., Doty, S.D., van Dishoeck, E.F. et al. 2003, A&A, 406, 937

Brinch, C., & Hogerheijde, M.R. 2010, A&A, 523, A25

Bruderer, S., Benz, A. O., Doty, S. D., van Dishoeck, E. F., & Bourke, T. L. 2009, ApJ, 700, 872

Bruderer, S., et al. 2010, A&A, 521, L44

Bruderer, S., Benz, A. O., Stäuber, P., & Doty, S. D. 2010, ApJ, 720, 1432

Caselli, P., Keto, E., Pagani, L. et al. 2010, A&A, 521, L29

Cernicharo, J., & Crovisier, J. 2005, Space Science Reviews, 119, 29

Chavarría, L., et al. 2010, A&A, 521, L37

Codella, C., et al. 2010, A&A, 518, L112

van Dishoeck, E.F., Kristensen, L.E., Benz, A.O. et al. 2011, PASP, 123, 138

Dominik, C., Ceccarelli, C., Hollenbach, D., & Kaufman, M. 2005, ApJL, 635, L85

Fich, M., et al. 2010, A&A, 518, L86

Franklin, J., Snell, R.L., Kaufman, M.J. et al. 2008, ApJ, 674, 1015

Gerin, M., et al. 2010, A&A, 518, L110

Giannini, T., Nisini, B., & Lorenzetti, D. 2001, ApJ, 555, 40

de Graauw, T., Helmich, F.P., Phillips, T.G. et al. 2010, A&A, 518, L6

Johnstone, D., Fich, M., McCoey, C. et al. 2010, A&A, 521, L41

Lefloch, B., et al. 2010, A&A, 518, L113

Keto, E., & Caselli, P. 2010, MNRAS, 402, 1625

Kaufman, M.J., & Neufeld, D.A. 1996, ApJ, 456, 611

Kaufman, M. J., Wolfire, M. G., Hollenbach, D. J., & Luhman,
     M. L. 1999, ApJ, 527, 795

van Kempen, T.A., Kristensen, L.E., Herczeg, G.J. et al. 2010,
     A&A, 518, L121

Kristensen, L.E., Visser, R., van Dishoeck, E.F. et al. 2010, A&A,
     521, L30

Kristensen, L.E. et al. in prep.

Marseille, M. G., et al. 2010, A&A, 521, L32

Melnick, G. J. 2009, Submillimeter Astrophysics and Technology:
     a Symposium Honoring Thomas G. Phillips, 417, 59

Menten, K. M., Wyrowski, F., Belloche, A., Güsten, R., Dedes, L.,
     Müller, H. S. P. 2011, A&A, 525, A77

Neufeld, D. A., et al. 2009, ApJ, 706, 170

Nisini, B., et al. 2010, A&A, 518, L120

Poglitsch, A., Waelkens, C., Geis, N. et al. 2010, A&A, 518, L2

Roberts, H., & Millar, T. J. 2007, A&A, 471, 849

Stäuber, P., Doty, S. D., van Dishoeck, E. F., Jørgensen, J. K., &
     Benz, A. O. 2004, A&A, 425, 577

Stäuber, P., Doty, S. D., van Dishoeck, E. F., & Benz, A. O. 2005,
     A&A, 440, 949

Stäuber, P., Benz, A. O., Jørgensen, J. K., van Dishoeck, E. F.,
     Doty, S. D., & van der Tak, F. F. S. 2007, A&A, 466, 977

van der Tak, F. F. S., et al. 2010, A&A, 518, L107

Visser, R. et al. in prep.

van der Werf, P. P., et al. 2010, A&A, 518, L42

Wyrowski, F., et al. 2010, A&A, 521, L34

Wyrowski, F., Menten, K. M., Güsten, R., & Belloche, A. 2010,
     A&A, 518, A26